Coherent imaging of biological samples with femtosecond pulses at the free-electron laser FLASH

2010 New J. Phys. 12 035003

(http://iopscience.iop.org/1367-2630/12/3/035003)

New Journal of Physics
The open-access journal for physics

Coherent imaging of biological samples with femtosecond pulses at the free-electron laser FLASH

A P Mancuso[1], Th Gorniak[2], F Staier[2], O M Yefanov[1], R Barth[2], C Christophis[2], B Reime[1], J Gulden[1], A Singer[1], M E Pettit[3], Th Nisius[4], Th Wilhein[4], C Gutt[1], G Grübel[1], N Guerassimova[1], R Treusch[1], J Feldhaus[1], S Eisebitt[5], E Weckert[1], M Grunze[2,6], A Rosenhahn[2,7] and I A Vartanyants[1,7]

[1] Deutsches Elektronen-Synchrotron DESY, Notkestraße 85, D-22607 Hamburg, Germany
[2] Angewandte Physikalische Chemie, Universität Heidelberg, Im Neuenheimer Feld 253, D-69120 Heidelberg, Germany
[3] School of Biosciences, University of Birmingham, Birmingham B15 2TT, UK
[4] Institute for X-ray-Optics, RheinAhr-Campus Remagen, FH Koblenz, Südallee 2, D-53424 Remagen, Germany
[5] Institut für Optik und Atomare Physik, Technische Universität Berlin, Straße des 17 Juni 135, D-10623 Berlin, Germany
[6] Institute of Toxicology and Genetics, Forschungszentrum Karlsruhe, ITG, Bldg. 305, PO Box 3640, D-76021 Karlsruhe, Germany
E-mail: rosenhahn@uni-heidelberg.de and ivan.vartaniants@desy.de

New Journal of Physics **12** (2010) 035003 (14pp)
Received 22 September 2009
Published 31 March 2010
Online at http://www.njp.org/
doi:10.1088/1367-2630/12/3/035003

Abstract. Coherent x-ray imaging represents a new window to imaging non-crystalline, biological specimens at unprecedented resolutions. The advent of free-electron lasers (FEL) allows extremely high flux densities to be delivered to a specimen resulting in stronger scattered signal from these samples to be measured. In the best case scenario, the diffraction pattern is measured *before* the sample is destroyed by these intense pulses, as the processes involved in radiation damage may be substantially slower than the pulse duration. In this case, the scattered signal can be interpreted and reconstructed to yield a faithful image of the sample at a resolution beyond the conventional radiation damage limit. We employ coherent x-ray diffraction imaging (CXDI) using the free-electron

[7] Author to whom any correspondence should be addressed.

LASer in Hamburg (FLASH) in a *non-destructive* regime to compare images of a biological sample reconstructed using different, single, femtosecond pulses of FEL radiation. Furthermore, for the first time, we demonstrate CXDI, in-line holography and Fourier transform holography (FTH) of the same unicellular marine organism using an FEL and present diffraction data collected using the third harmonic of FLASH, reaching into the water window. We provide quantitative results for the resolution of the CXDI images as a function of pulse intensity, and compare this with the resolutions achieved with in-line holography and FTH.

S Online supplementary data available from stacks.iop.org/NJP/12/035003/mmedia

Contents

1. Introduction

Imaging of biological samples is an important way to understand their structure and function. Optical, and in particular fluorescence microscopy, are the most common tools to study the structure and function of biological objects. Recent developments [1] have pushed the resolution of visible light microscopy approximately an order of magnitude beyond Abbe's diffraction limit [2]. These powerful methods all rely on the use of labels to mark the biological structures of interest. Using green fluorescent protein, researchers can watch previously invisible processes *in situ* and *in vivo*, including the development of nerve cells in the brain or how cancer cells spread [3]. However, one fundamental deficit of all these methods is that the non-labeled and non-fluorescent environment of the molecular systems under study remains invisible. Soft x-rays [4, 5] and electrons [6] do not need molecular labels and are well suited for imaging whole biological samples. Electron microscopy achieves the highest resolution; however, the samples require particular preparation due to their limited penetration depth. X-rays, especially at the water window, can produce high contrast images of non-crystalline biological samples, e.g. cells, in their natural environment which is extremely important for understanding their functionality [7, 8]. In both electron and x-ray imaging, resolution is limited by the quality of the optics used, incident flux and radiation damage [9, 10] caused in biological samples.

A new approach to overcome these difficulties is based on the use of ultrashort pulses of x-ray free-electron lasers (XFEL) [11]–[13]. An elegant idea is based on measuring a sufficiently sampled diffraction pattern from a series of biological specimens (e.g. viruses or even molecules) each illuminated by single, femtosecond free-electron lasers (FEL) pulses [14]. This approach circumvents the conventional radiation damage limit of imaging biological samples by measuring the elastically scattered signal before radiation damage destroys the sample. Femtosecond single-pulse imaging was recently demonstrated [15, 16] at the Free-electron LASer in Hamburg (FLASH) facility at DESY in Hamburg [17]. To obtain a three-dimensional (3D) image of a biological sample with subnanometer spatial resolution diffraction images of many *reproducible* copies, or at least reproducible subunits, will need to be recorded to get a sufficient signal-to-noise ratio for each projection. Injecting single particles in the ultra-bright FEL beam for most *non-reproducible* biological samples, e.g. cells, will give the same 2D information as for samples supported on membranes. The latter approach is much easier to implement in practice and can be combined with well-established cryo-cooling techniques. This is particularly pertinent for membrane proteins that in general do not form 3D crystals, but can form 2D crystals [18]. In our previous work, we have shown a first demonstration of single train FEL coherent imaging for a 2D, finite crystalline structure [19]. Furthermore, some pioneering results on coherent imaging of cells and viruses supported by membranes have been reported recently [20]–[23]. Here, we report on coherent x-ray diffraction imaging (CXDI), in-line holography and Fourier transform holography (FTH) performed with femtosecond coherent pulses of FLASH on critical point dried biological objects supported on a silicon nitride membrane.

FLASH, providing up to 10^{13} coherent photons in a single femtosecond pulse, is a unique source for coherent imaging techniques. CXDI is based on the idea of illuminating a finite object with a coherent beam and measuring a sufficiently sampled diffraction pattern originating from this object [24]–[27] (figure 1). Iterative phase retrieval techniques [28]–[30] are applied to reconstruct the structure of the object. This approach produces reliable images; however, significant computational time is required to obtain high quality images. Due to its lensless approach, CXDI has the potential to produce diffraction limited images, not limited by the quality of optics. Digital in-line holography [31, 32] and FTH [33]–[35] are based on using a reference wave that originates from a pinhole or scatterer located either in front of the sample (in-line holography), or in the plane of the sample (FTH) (figure 1). As a result, the phase problem can be solved without ambiguity, but with additional restrictions on spatial resolution imposed by the generation of the reference wave. Digital in-line holography has recently been demonstrated for the first time with an FEL source [36]. Moreover, a coherent imaging reconstruction, by CXDI or holography, is actually a representation of the complex-valued exit wave function of the object with the magnitude describing the transmission through the sample and the phase describing the refraction due to the sample. Thus, a coherent imaging reconstruction yields an image with more information than just absorption contrast [25, 37].

2. Experimental procedure

Our coherent imaging experiment was performed at FLASH tuned to produce a fundamental photon wavelength of 8 nm and delivered to the PG2 monochromator beamline (see appendix). This beamline allows access to the fundamental and higher harmonic FEL radiation and hence to perform experiments in the water window. FLASH produced about 10 fs pulses with 15–20 μJ

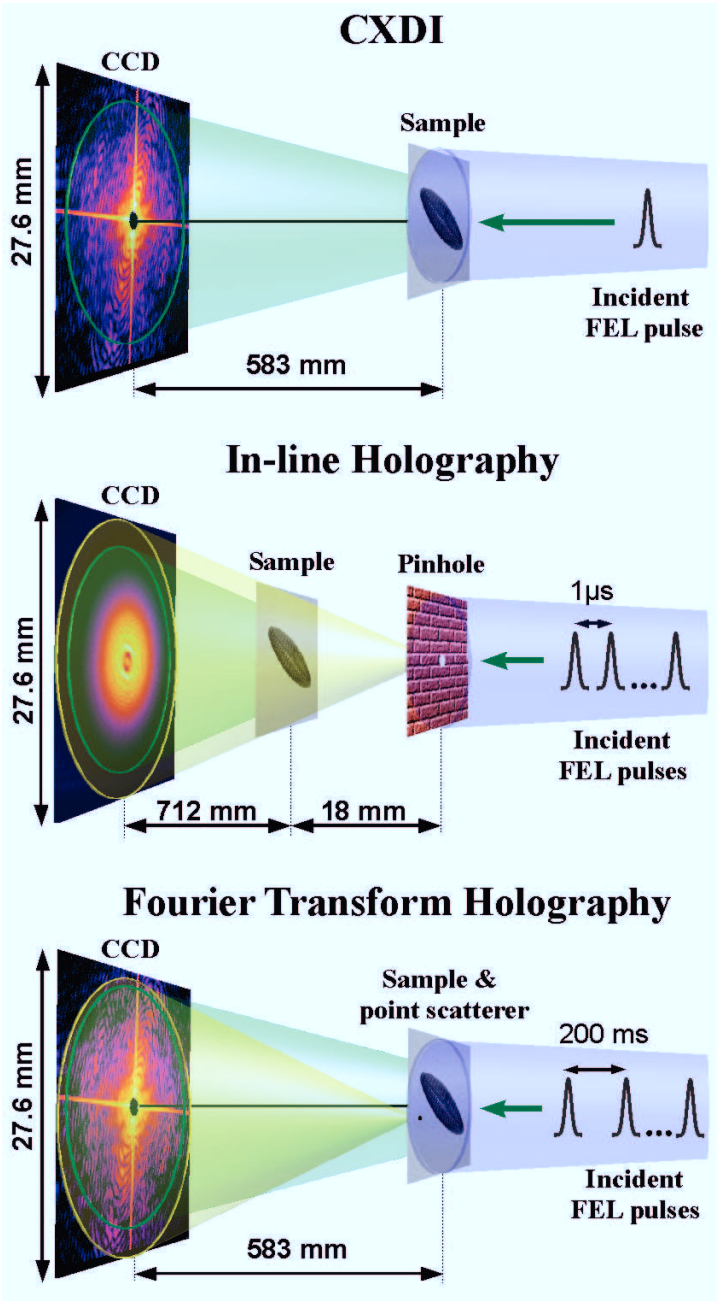

Figure 1. Schematic view of the different imaging experiments using coherent beams. (Top panel) CXDI experiment: a single pulse from the FEL first interacts with the sample, and then the diffracted radiation propagates to a CCD detector. (Middle panel) In-line holography experiment: single pulses from the FEL first scatter on the pinhole, then part of the reference beam interacts with the sample, and then the interference pattern is measured on a CCD detector. (Bottom panel) FTH experiment: single pulses from the FEL interact with the sample and reference point scatterer resulting in an interference pattern measured on a CCD detector.

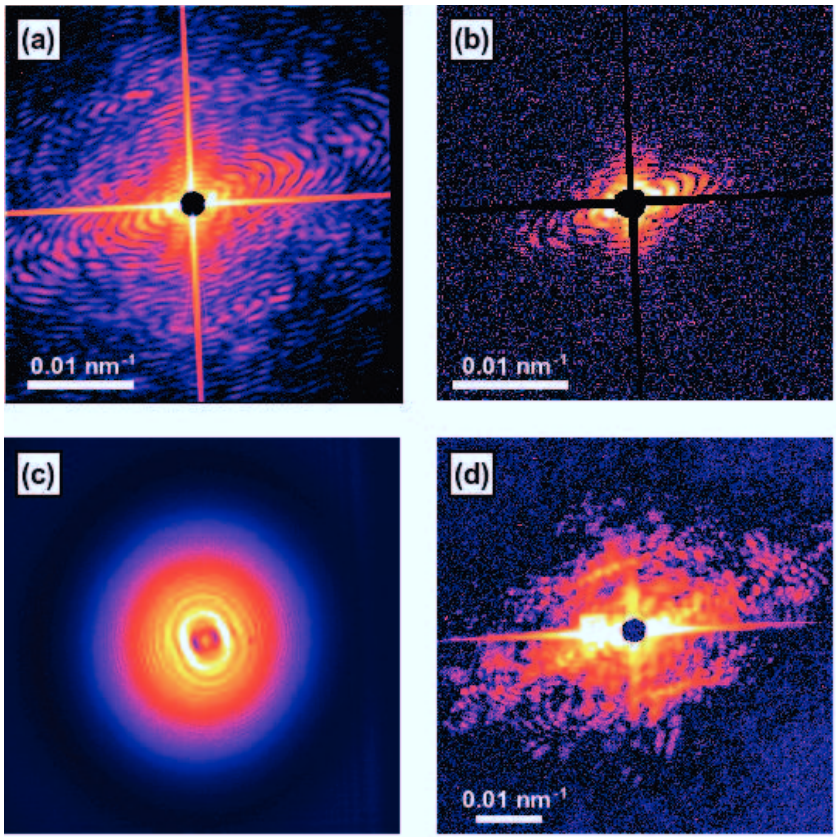

Figure 2. Results of the coherent imaging experiment. (a) CXDI experiment. The sum of ten accumulated (30 s each) diffraction patterns measured at fundamental 8 nm wavelength. (b) The same as (a) for a single FEL pulse measurement with streaks and beamstop removed (see the appendix for details). (c) In-line holography diffraction pattern accumulated for 8 s. (d) Diffraction pattern measured at the third harmonic of the fundamental wavelength (2.66 nm) accumulated for 300 s. A nonlinear color scale is used to display these data. Logarithmic scale is used in (a, b, d).

power per pulse in the fundamental. Diffraction data were recorded using single pulses of the fundamental FEL radiation scattered from a diatom, *Navicula perminuta.* Diatoms are unicellular algae in which the protoplast is encased in a silica cell wall (see the appendix). An average of 9×10^9 photons per pulse (estimated by ray tracing) was delivered to a focal spot of 50 μm full width at half maximum (FWHM) in a dedicated vacuum chamber (see the appendix). About 2.5×10^8 photons per average pulse are then incident on the $10 \times 5\ \mu m^2$-sized sample. In similar experiments [19], we have observed that the coherence length in the focal plane was significantly greater than 10 μm, which is sufficient to coherently illuminate our sample. Fifty different single-pulse diffraction patterns were recorded from the same diatom. A movie of these diffraction patterns is included in the supplementary material, available from stacks.iop.org/NJP/12/035003/mmedia. Additionally, a series of ten multiple pulse measurements, each of 30 s duration, was recorded. The sum of these exposures (1500 pulses in total) is shown in figure 2(a). A typical diffraction pattern collected using a single pulse is shown in figure 2(b). The high contrast in these diffraction patterns indicates sufficient

coherence length. Note the difference in signal between these data sets, especially far from the center of the patterns that corresponds to higher momentum transfer, which determines the resolution of the reconstructed image [19].

3. Image reconstruction

3.1. CXDI

Figure 3(a) shows the CXDI reconstruction from the integrated measurement, whereas figures 3(b)–(d) show reconstructions from different single-pulse measurements. The reconstructions in figure 3 were obtained by applying the guided hybrid input–output (GHIO) [30] algorithm (see the appendix). Due to the self-amplified spontaneous emission (SASE) process [38] individual femtosecond pulses are statistically different. Comparing results for the same sample illuminated by different single pulses (figures 3(b)–(d)) we see identical features imaged at different resolutions, dependent on the pulse intensity. This demonstrates that statistical pulse to pulse variations of a SASE FEL do not represent a limitation for coherent imaging for the resolutions achieved here. The reconstruction from the integrated measurement clearly provides the most detailed information about the diatom. We estimate that the resolution of this reconstructed image is 380 nm. In this case, the reconstructed resolution is limited by the size of the detector and not by the signal-to-noise ratio. Comparing the reconstructed far-field intensities with a modulation transfer function (MTF) for an incoherent imaging system [2], we estimate that if the detector was larger we would reconstruct an image of the diatom up to 225 nm resolution from this measurement. Similar calculations give a resolution of 650 nm for the brightest single shot image, and 1200 nm for the weakest single shot image analyzed (see the appendix). In this case, the resolution is limited by the signal-to-noise ratio at high q-values, which is clearly a function of the incident coherent flux.

The same diatom was also measured with the third harmonic radiation of FLASH, corresponding to a wavelength of 2.66 nm. This wavelength is in the so-called water window. In these measurements, the incident flux was significantly less due to the smaller fraction of third harmonic radiation in the beam (about 0.5% of the total beam flux), and the reduced transmission of the beamline at these energies. Consequently, 3.5×10^6 photons per pulse were available at the end station under these conditions (see the appendix). With this photon flux single-pulse measurements were not feasible. We have measured integrated diffraction patterns at these energies from ten exposures each of 30 s duration with FLASH delivering 30 pulses per pulse train at 5 Hz pulse train repetition rate (4500 pulses per exposure). The measured diffraction pattern is shown in figure 2(d) scattering to a resolution of 230 nm. Examination of this diffraction pattern unexpectedly reveals poorer contrast compared with the integrated and single-shot diffraction patterns produced using the fundamental radiation (figures 2(a) and (b)). We attribute this reduction to a significantly reduced coherence length of the radiation at the third harmonic, which becomes smaller than the size of our diatom along its major axis. As a result, the reconstruction of an image from this third harmonic diffraction pattern was not possible.

3.2. In-line holography

The same *N. perminuta* diatom was imaged by digital in-line holography. In order to obtain the divergent wavefront necessary for in-line holography, a pinhole was used as a spatial filter

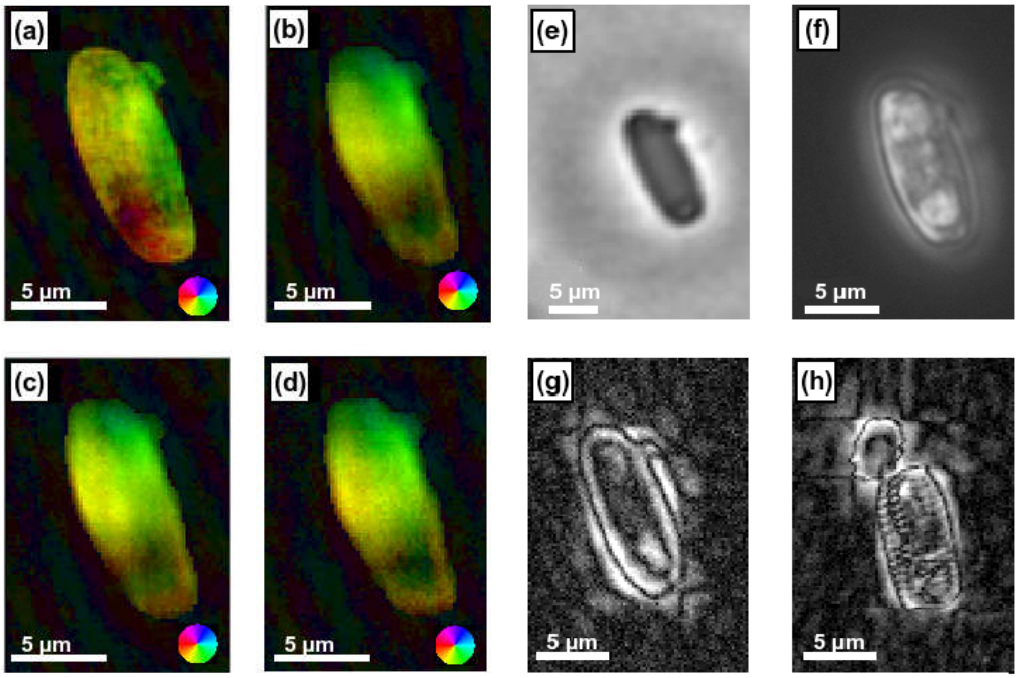

Figure 3. (a)–(d) Reconstruction from the CXDI data. (a) Reconstructed image of a cell of *N. perminuta* from the integrated diffraction pattern (figure 2(a)). (b)–(d) Same from the different single-pulse diffraction patterns. (e) In-line holography reconstruction from the diatom cell. (f) Optical micrograph of the *Navicula* cell (20×, NA 0.45). (g) Reconstructed Fourier transform hologram of the diatom sample. (h) FTH reconstruction of a different *N. perminuta* cell. In (a)–(d), a color scale with the magnitude encoded in the value and the phase encoded in the hue of the image is implemented. The phase colormap is given by the wheel in the bottom right corner of the images.

(figure 1). Fitting the measured intensity profile of the Airy pattern determines the effective diameter of the pinhole to be $A = 1.14\,\mu$m. Considering that the focal spot size is significantly larger than the pinhole, the flux behind the pinhole is estimated to be 0.04% of the total flux. This reduces the flux incident on the sample to 3.6×10^6 photons per pulse. In contrast to the CXDI results given above, where the measured momentum transfer range determines the resolution, the theoretical resolution here is determined by the effective numerical aperture (NA) resulting from the illumination of the detector by the central maximum of the Airy disc [32]. With our geometry, the effective NA was 0.0086, leading to a theoretical resolution of 570 nm. The hologram shown in figure 2(c) is the drift corrected sum of eight 1 s exposures, each containing five pulse trains of 30 single pulses. In figure 3(e), the in-line holographic reconstruction of the diatom is shown. An optical microscope image of the diatom is given in figure 3(f) for comparison. Line profile analysis by the 10–90% criterion of the diatom and the reconstruction of a H1299 cell (see the appendix) indicates an experimental resolution of ∼950 nm. Due to the long exposure times pointing instabilities in the beam led to uniaxial smoothing, which leads to a resolution that is worse than expected. For the in-line holography experiment no beamstop

was used. Thus, low-frequency information about the object is encoded in the hologram and present in the reconstruction. This allows quantitative assessment of the x-ray attenuation.

3.3. FTH

In addition to the CXDI and in-line holographic reconstructions, FTH was also possible with the same diatom. An inverse Fourier transform was applied to the integrated CXDI measurements shown in figure 2(a). Unknown at the time of measurement, a point scatterer was present in the beam near the diatom. Consequently, the inverse transform yielded an FTH reconstructed image of the diatom shown in figure 3(g) and that of a second diatom shown in figure 3(h). It can be seen that predominantly edge information about the diatoms is reconstructed, including the well-resolved 'rib'-like structure with a period of 550 nm easily visible in figure 3(h). This can be explained by the absence of low-frequency data, due to the presence of the beamstop, leaving only higher spatial frequency information to be reconstructed. It is difficult to quantify the reference-limited resolution of this reconstruction as the point scatterer has not been characterized prior to the experiment. Based on conservative resolution estimates (see the appendix) we can say that the resolution obtained in FTH is better than 450 nm.

3.4. Comparison of coherent imaging techniques

Ultimately, it is interesting to compare the real space resolution and different contrast obtained for each imaging technique. We see high quality edge information from a Fourier transform hologram, similar edge information and opacity from in-line holography, and phase information, describing the sample's refractive effects, from CXDI. Unsurprisingly, the FTH and integrated CXDI images, with the same incident flux, produce images with similar resolutions. The resolution from in-line holography was poorer, but required a much lower incident flux of only 4.3×10^7 photons on the sample area. The brightest measured single pulse CXDI case used approximately 1.6×10^9 photons incident on the sample area to produce a 650 nm resolution real space image of the diatom cell. The integrated case required $\sim 3.7 \times 10^{11}$ photons to deliver a possible ultimate resolution of 225 nm. These measurements concord roughly with the expected behavior that the resolution achievable scales as the fourth power of the scattered intensity [10]. By optimizing the beamline optics to improve transmission at these energies we could expect, in principle, to have 10^{12}–10^{13} coherent photons per pulse on the sample area. With this available flux, using the aforementioned scaling law, a resolution of up to 60 nm could be expected for single-pulse imaging of similar biological samples.

4. Conclusions

In summary, we have demonstrated single-pulse, femtosecond coherent diffractive imaging for a single-celled organism (a diatom) supported by a membrane. We have verified that images reconstructed using CXDI are similar for different FEL pulses, and that the resolution achievable scales roughly as the fourth power of the intensity of the pulse. By imaging the same biological sample with different single pulses of FLASH below the radiation damage limit we, for the first time, demonstrate the possibility to reconstruct identical features in a sample illuminated by statistically different FEL SASE pulses. These results are especially important for the success of single-particle imaging of reproducible samples injected into an FEL beam and imaged by

different FEL pulses. We also demonstrate here, for the first time, a comparison of different coherent imaging techniques using an FEL applied to the same sample of *N. perminuta*. We can clearly see the qualitative differences in the images, and also compare the resolutions obtained as a function of flux. Furthermore, we have shown a CXDI measurement using a higher harmonic of FLASH that extends into the water window. From our investigation it is reasonable to expect that with future, shorter wavelength XFEL sources it will be possible to make single-pulse CXDI measurements in the water window to resolutions of tens of nanometers, opening the way to biological imaging that circumvents the conventional radiation damage limit.

Acknowledgments

The H1299 cell line was kindly provided by U Alon (Weitzmann Institute). The Heidelberg authors kindly acknowledge financial support from the BMBF projects 05KS4VH1 and 05KS7VH1. The work was supported by the 6th framework EU integrated project AMBIO. We are greatly indebted to the scientific and technical team at FLASH, in particular the machine operators and run coordinators, being the foundation of the successful operation and delivery of the SASE-FEL beam.

Appendix A. Materials and methods

A.1. FLASH operation conditions and PG2 beamline

FLASH [17, 39] was operated with a fundamental wavelength of 8 nm in a single-bunch operation mode, with a bunch repetition rate of 5 Hz. The average pulse energy after two 1 mm apertures in the tunnel (about 16.3 and 20.8 m behind the last undulator, respectively), which were used to reduce the contribution of incoherent spontaneous radiation and background radiation, was 3 μJ which is equivalent to 2×10^{11} photons per pulse at the source. Accounting for beamline transmission this results in 9×10^9 photons per pulse at the endstation. For the third harmonic experiments FLASH was operated with 30 pulses per train. Accounting for the lower fraction of the third harmonic component in the FEL beam ($\sim$0.5%) and lower beamline transmission at this wavelength we find we had about 3.5×10^6 photons per pulse in this case. PG2 [40] is a plane grating monochromator beamline with the last mirror of the beamline being a focusing mirror with a focal length of 2 m, which provides an image of the source. From downstream measurements we estimate a beam size in the focal plane of the order of 50 μm FWHM in the horizontal and vertical directions for the zeroth order beam and 50 μm $\times$ 1 mm FWHM for the third harmonic beam.

A.2. Samples

N. perminuta algal cultures were grown according to known protocols [41, 42] and resuspended in artificial sea water (ASW). Cells of *Navicula* were allowed to attach to 30 nm thick silicon nitride membranes for 1 h. The samples were fixed in 2.5% glutaraldehyde for 30 min and the ASW was exchanged for distilled water in three steps. The cell water was slowly exchanged for ethanol by six different ethanol/water concentrations and the cells were finally critical point dried (Bal-Tec CPD 030). Diatom cells are encased in two silica shells called the frustule [43]. The elemental composition of diatoms varies with species, available nutrients and season [44].

Silica contents between 4 and 50% of dry weight are reported and a range of organic compounds are present (e.g. carbohydrates, proteins) [44]. Diatom frustules not only fascinate the human eye because of their arresting symmetry, but also reveal remarkable mechanical properties which are suggested to have evolved as effective armor against predators [45]. In this study, the fine structure of the frustle was used to estimate the resolution reached in FTH.

H1299 cells (derived from human lung carcinoma tissue) were cultivated on fibronectin coated Si_3N_4 membranes for 12 h in Roswell Park Memorial Institute (RPMI 1640) supplemented with 10% fetal bovine serum (FBS) and 1% L-glutamine, all purchased at Gibco. After fixation with 2.5% paraformaldehyde in PBS, the cell water was slowly exchanged for ethanol by six different ethanol/water concentrations and the cells were finally critical point dried (Bal-Tec CPD 030).

A.3. Experimental apparatus

The experiment was conducted in a dedicated HORST (HOlographische RöntgenSTreuapparatur) vacuum chamber [46], which was connected to the PG2 beamline at FLASH. The HORST chamber consists of an upstream shutter, a sample stage, and a flight tube to the charged-coupled device (CCD) at the most downstream position. Inside 13 translation stages are mounted on an optical table which allows positioning of samples, spatial filters and the camera with submicrometer accuracy in order to adjust all elements to the optimal imaging geometry. This chamber contains all the flexibility required to perform both in-line holography and coherent imaging and to adapt the experimental geometry during the experiment without breaking the chamber vacuum.

The 8 nm FEL beam delivered to beamline PG2 was incident on the sample at a distance of approximately 71.5 m from the source. In the CXDI and FTH geometry, the diffracted radiation propagated from the sample 583 mm to the detector (in-vacuum CCD LOT/Andor DODX436-BN with 2048 × 2048 pixels, each 13.5 μm square with 16-bit digitization). For digital in-line holography a pinhole with a diameter of $A = 1.2\ \mu$m was inserted upstream of the sample plane to create a divergent light cone which was then incident on the samples and propagated to the detector positioned 730 mm downstream of the pinhole (see figure 1). For the in-line holography experiment the *N. perminuta* diatoms were positioned 18 mm, and the H1299 cells 10 mm, downstream of the beam-defining pinhole.

A.4. CXDI image reconstruction

In order to increase the signal-to-noise ratio [19], the collected diffraction patterns were binned in each dimension by a factor of 8. The support used in all reconstructions was obtained by applying the HIO [28] algorithm to the integrated data. The images shown in figure 3(a)–(d) are an average of 20 images that have been reconstructed using this fixed tight support and the binned diffraction patterns using the GHIO algorithm [30] with eight seeds and five generations each of 1000 iterations. Note the relatively small beamstop region in figures 2(a) and (b), which covers just more than one speckle in the diffraction pattern. As such, this small region of missing data is not expected to affect the reconstruction process. Similarly, the bright cross across the diffraction pattern (due to scattering from the supplementary membrane window) is approximately the width of a single speckle. These data, along with the beamstop data, are removed from the pattern and allowed to remain unconstrained in the reconstruction process.

A.5. Evaluation of resolution in CXDI experiments

The integrated image resolution was limited by the detector size and position; however, the single-shot reconstructions are limited in resolution by the significantly lower signal contained in a single shot. The first single-shot reconstruction shown (in figure 3(b)) exhibits the highest fidelity of the three highlighted in this paper. The second (figure 3(c)) and third (figure 3(d)) reconstructions shown are also reconstructed from single-shot data, and coincide very well with the first reconstruction's general features. These images were reconstructed from single-shot diffraction patterns of 80 and 84% of the first shot's intensity value, respectively. A fourth single shot image (not shown in figure 3), with much lower total intensity (∼44%) than these first three cases, has also been analyzed (the evaluation of its resolution is shown in figure A.1(a)). These lower intensity measurements necessarily result in lower quality reconstructions, though we observe little visible difference between figures 3(b), (c) and (d) where the intensities in each pattern are similar in magnitude.

To quantify the difference between different single-shot reconstruction images we define a difference coefficient D_{ij}

$$D_{ij} = \frac{\sum |\rho_i - \rho_j|}{\sum |\rho_i + \rho_j|},$$

where ρ_{ij} is the normalized magnitude of the reconstructed wavefield, i and j subscript the particular data set and summation is made by the pixels of the support region. We find the reconstructions of the second and third data sets, being most alike in diffracted intensity (only differing by 5%), are also most similar with $D_{23} = 0.057$. The first reconstruction, derived from a significantly higher intensity diffraction pattern, unsurprisingly differs more from reconstructions 2 and 3 with $D_{12} = 0.074$ and $D_{13} = 0.071$. The reconstruction from the weakest data set differs most markedly with $D_{14} = 0.107$.

We evaluate the resolution of each of our CXDI reconstructed images by plotting the radial average of the ratio $I_{\text{recon}}(q)/I_{\text{meas}}(q)$, where $I_{\text{recon}}(q)$ are the reconstructed far-field intensities and $I_{\text{meas}}(q)$ the corresponding measured intensities as described in [20]. The difference between single-pulse measurements is clear in figure A.1(a), where we see the highest intensity pulse exhibits features to a higher resolution (650 nm) than the lowest intensity pulse (1200 nm). The other pulses fall in between in order of their intensity, but are not shown in this diagram for clarity. These resolution values have been determined by comparing the expression $\langle I_{\text{recon}}(q)/I_{\text{meas}}(q)\rangle$ with an MTF [20] for a radially symmetric incoherent imaging system with 80% efficiency (see figure A.1(b)). The cutoff of this MTF is considered to be the resolution of the reconstructed image.

A.6. Evaluation of FTH and in-line holographic resolution

As mentioned above, the silica cell wall of the *N. perminuta* cells shows a hole pattern with different periodicity in the respective perpendicular directions. Scanning electron microscopy images of similar diatoms (not shown) reveal a feature size of 300 and 550 nm, respectively. In the FTH reconstruction, the rib-like structure of the larger features is well resolved (horizontal lines in figure 3(h)), whereas the smaller connecting bars are not visible. Therefore, we conservatively estimate the resolution in FTH to be 450 ± 50 nm. The FTH reconstruction used linear interpolation to fill in the missing regions of data corresponding to the beamstop and the streaks.

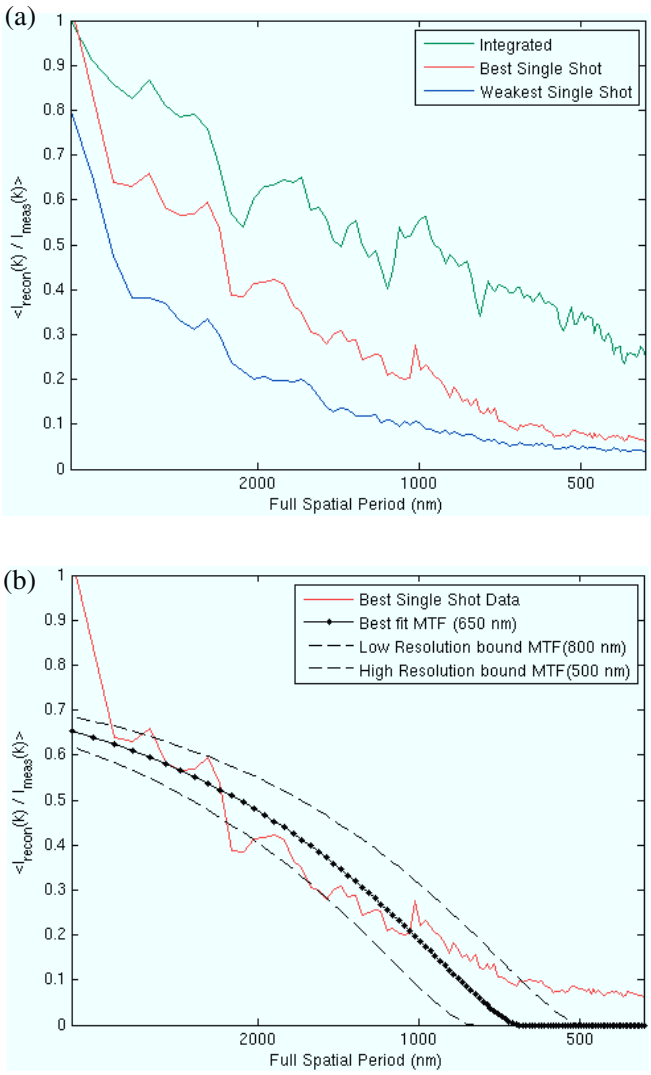

Figure A.1. (a) Radial average of the ratio of the far-field reconstructed and measured intensities for the integrated measurement (green line), the brightest single-pulse measurement (red line) and the weakest single-pulse measurement (blue line). (b) Radial average of the ratio of the far-field reconstructed and measured intensities for the brightest single shot, as above (red line), a fit to this measurement with an MTF of an ideal incoherent imaging system with 80% efficiency and a resolution of 650 nm (black solid line), upper and lower bounds with similar MTFs of resolution 800 and 500 nm, respectively (black dashed lines). Full spatial period indicates $2\pi/q$, where q is the momentum transfer in the diffraction image.

For the in-line holography experiment no beamstop was used and low-frequency information about the object is encoded in the hologram and present in the reconstruction. The experimental resolution in digital in-line holography was determined by analyzing the 10–90% contrast change in line-profiles of the reconstruction of the diatom and the H1299 cell (shown in figure A.2) to be 950 nm. This is poorer than theoretically predicted. A more

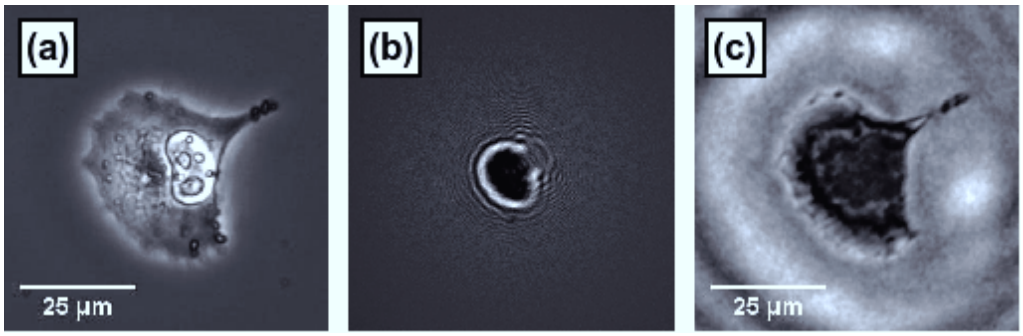

Figure A.2. Images of a H1299 cell. (a) Optical micrograph (20× objective, NA 0.45). (b) Accumulated in-line hologram as a drift-corrected sum of 10 exposures, each having an exposure time of 1 s. High-frequency interference fringes are visible. (c) Reconstruction of (b). The outline of the cell as well as internal structure can be correlated with (a). Note the difference in contrast between VUV radiation and visible light.

detailed analysis reveals that the holograms are randomly shifted along the diagonal of the detector by a magnitude of ∼15 pixels from exposure to exposure. The reason might either be vibration of the sample stage (then the shift of 15 pixels at the detector equals a travel of the sample of about 5 μm) or a result of the pointing instability of the FEL beam (with a change in pointing direction of 0.016° or 0.28 mrad), as the SASE process can start at different places within the electron bunches. Since the translation stages used in the experimental setup have a travel accuracy in the submicrometer range, it is unlikely that vibrations of the sample stage can be the only cause of the shift of the diffraction pattern. We rather assume that the shift is due to the aforementioned pointing instability of the FEL beam and associated amplifications along the optical path. The shift between different exposures was corrected for by aligning to fiducial features before summing up the individual exposures. However, since each obtained hologram is an accumulation over several pulses, the shift cannot be eliminated completely and may be the reason for the loss of the finest interference fringes and thus the decrease in resolution.

References

[1] Hell S W 2007 *Science* **316** 1153
[2] Goodman J W 1986 *Introduction to Fourier Optics* (New York: McGraw-Hill)
[3] The Nobel Prize in Chemistry 2008 Press Release, 8 October 2008
[4] Le Gros M A *et al* 2005 *Curr. Opin. Struct. Biol.* **15** 593
[5] Donoghue P C J *et al* 2006 *Nature* **442** 680
[6] Frank J (ed) 2006 *Electron Tomography: Methods for Three-Dimensional Visualization of Structures in the Cell* 2nd edn (New York: Springer)
[7] Meyer-Ilse W *et al* 2001 *J. Microsc.* **201** 395
[8] Parkinson D Y, McDermott G, Etkin L D, Le Gros M A and Larabell C A 2008 *J. Struct. Biol.* **162** 380
[9] Henderson R 2004 *Q. Rev. Biophys.* **37** 3
[10] Howells M R *et al* 2009 *J. Electron Spectrosc. Relat. Phenom.* **170** 4
[11] Emma P *et al* 2009 http://www-ssrl.slac.stanford.edu/lcls/commissioning/documents/th3pbi01.pdf

[12] Tanaka T and Shintake T (ed) 2005 *SCSS X-FEL Conceptual Design Report* SCSS XFEL RIKEN 679-5148 (http://www-xfel.spring8.or.jp/)
[13] Altarelli M *et al* (ed) 2006 *XFEL Technical Design Report* DESY 2006-097 (http://xfel.desy.de/tdr/index_eng.html)
[14] Neutze R, Wouts R, van der Spoel D, Weckert E and Hajdu J 2000 *Nature* **406** 752
[15] Chapman H N *et al* 2006 *Nat. Phys.* **2** 839
[16] Chapman H N *et al* 2007 *Nature* **448** 676
[17] Ackermann W *et al* 2007 *Nat. Photonics* **1** 336
[18] Uzgiris E E and Kornberg R D 1983 *Nature* **301** 125
[19] Mancuso A P *et al* 2009 *Phys. Rev. Lett.* **102** 035502
[20] Shapiro D *et al* 2005 *Proc. Natl Acad. Sci. USA* **102** 15343
[21] Song C, Jiang H, Mancuso A, Amirbekian B, Peng L, Sun R, Shah S S, Hong Zhou Z, Ishikawa T and Miao J 2008 *Phys. Rev. Lett.* **101** 158101
[22] Williams G J *et al* 2008 *Cytometry* **73A** 949–57
[23] Nishino Y *et al* 2009 *Phys. Rev. Lett.* **102** 018101
[24] Miao J, Charalambous P, Kirz J and Sayre D 1999 *Nature* **400** 342
[25] Pfeifer M A, Williams G J, Vartanyants I A, Harder R and Robinson I K 2006 *Nature* **442** 63
[26] Thibault P, Dierolf M, Menzel A, Bunk O, David C and Pfeiffer F 2008 *Science* **321** 379
[27] Abbey B, Nugent K A, Williams G J, Clark J N, Peele A G, Pfeifer M A, de Jonge M and McNulty I 2008 *Nat. Phys.* **4** 3948
[28] Fienup J R 1982 *Appl. Opt.* **21** 2758
[29] Elser V 2003 *J. Opt. Soc. Am.* A **20** 40
[30] Chen C C, Miao J, Wang C W and Lee T K 2007 *Phys. Rev.* B **76** 064113
[31] Lindaas S, Howells M, Jacobsen C and Kalinovsky A 1996 *J. Opt. Soc. Am.* A **13** 1788
[32] Rosenhahn A, Barth R, Staier F, Simpson T, Mittler S, Eisebitt S and Grunze M 2008 *J. Opt. Soc. Am.* A **25** 416
[33] McNulty I, Kirz J, Jacobsen C, Anderson E H, Howells M R and Kern D P 1992 *Science* **256** 1009
[34] Eisebitt S, Lüning J, Schlotter W F, Lörgen M, Hellwig O, Eberhardt W and Stöhr J 2004 *Nature* **432** 885
[35] Stadler L-M, Gutt C, Autenrieth T, Leupold O, Rehbein S, Chushkin Y and Grübel G 2008 *Phys. Rev. Lett.* **100** 245503
[36] Rosenhahn A *et al* 2009 *Opt. Express* **17** 8220
[37] Gührs E, Günther C M, Könnecke R, Pfau B and Eisebitt S 2009 *Opt. Express* **17** 6710
[38] Saldin E L, Schniedmiller E A and Yurkov M V 2000 *The Physics of Free Electron Lasers* (Berlin: Springer)
[39] Tiedtke K *et al* 2009 *New J. Phys.* **11** 023029
[40] Wellhoefer M, Martins M, Wurth W, Sorokin A A and Richter M 2007 *J. Opt.* A **9** 749
[41] Pettitt M E, Henry S L, Callow M E, Callow J A and Clare A S 2004 *Biofouling* **20** 299
[42] Guillard R R L and Ryther J H 1962 *Can. J. Microbiol.* **8** 229
[43] Molino P J and Wetherbee R 2008 *Biofouling* **24** 365
[44] Lewin J C and Guillard R R L 1963 *Ann. Rev. Microbiol.* **17** 373
[45] Hamm C E, Merkel R, Springer O, Jurkojc P, Maier C, Prechtel K and Smetacek V 2003 *Nature* **421** 841
[46] Staier F 2009 *PhD thesis* Univerisität Heidelberg http://archiv.ub.uni-heidelberg.de/volltextserver/frontdoor.php?source_opus=9598